Chalcogenide Letters Vol. 19, No. 10, October 2022, p. 743 - 751

Physical properties and electronic structure of chalcogenide perovskite $BaZrS_3$ under pressure

G. M Zhang[a,b], S. Y. Li[a,*]
[a]*School of Artificial Intelligence, Nanchang Institute of Science and Technology, Nanchang, 330108, China*
[b]*Nanchang Industry and Technology School, Nanchang, 330108, China*

A theoretical comprehensive implementing of the structural, elastic, and electronic properties of chalcogenide perovskite $BaZrS_3$ under pressures 0 and 20 GPa is performed by ab-initio calculations included within the density functional theory (DFT). The lattice constants of the $BaZrS_3$ structure are well reproduced from our first-principles calculations, and in excellent agreement with experimental measurements. The electronic parameters indicate that the chalcogenide perovskite $BaZrS_3$ compound has a direct band gap of 1.75 eV. Moreover, the values of mechanical parameters, such as the elastic constant, increased under applied pressure. From the quotient of bulk to shear modulus of B/G, it is found that ductility becomes stronger with the increasing pressure, indicating pressure can effectively improve the ductility of the orthorhombic $BaZrS_3$.

(Received July 7, 2022; Accepted October 19, 2022)

Keywords: Chalcogenide perovskite, Electronic properties, Density functional theory, High pressure

1. Introduction

As a prototypical chalcogenide perovskite, $BaZrS_3$ perovskite is an ideal candidate for photovoltaic applications due to its suitable band gap of 1.76-1.85 eV, slightly higher than the optimum value for a single junction solar cell of 1.3-1.5 eV[1-2]. Due to their ferroelectric, piezoelectric, electrolytic, and optoelectronic properties enabling many advances in applications, chalcogenide perovskites have attracted significant attention[3]. Chalcogenide perovskites containing group-VI anions including S and Se are emerging as a novel class of semiconductors with potential photovoltaic and optoelectronic applications[4-6]. Thus, it timely to predict the behavior of this material under different pressures by use of theoretical research and analysis.

Moreover, high pressure processed chalcogenide perovskite materials have obtained many exhilarating results such as photoresponse enhancement, structural stability enhancement, bandgap optimization[7-8]. Recent investigation shows that the properties of $BaZrS_3$ is stable under exposure to air and moisture by measuring the X-ray diffraction and ultra-violet/visible absorption spectrum[9]. Kuhar *et al*. predicted a series of chalcogenide perovskites such as $SrSnSe_3$, $CaSnS_3$

* Corresponding author: lishaoyi2022@126.com
https://doi.org/10.15251/CL.2022.1910.743

and $SrSnS_3$ with tunable direct bandgaps within the optimal range of 0.9-1.6 eV for single junction solar cell applications[10]. To tune the band gap of chalcogenide perovskites, cation or anion alloying and dimensional reduction can be employed[10-11]. Nelson *et al* have reported experimental and theoretical studies of the Raman active phonons and the band-gap absorption edge in $BaZrS_3$, focusing on the effects of high pressure, and for the phonons also low temperature[12]. With the continuous emergence of various research methods for exploring photovoltaic materials in recent decades, high pressure technology has stood out as a clean and effective means. Such knowledge is key to evaluate the applicability of $BaZrS_3$ for thermoelectric and optoelectronic devices. To best of our knowledge, no theoretical and experimental studies were conducted to investigate the elastic, and electronic properties of $BaZrS_3$ under pressure. So, in this work, we have performed a comprehensive study on the structural, elastic, and electronic properties of the $BaZrS_3$ perovskite as a function of pressure using first-principles calculations based on density functional theory (DFT).

2. Calculation method

First-principles calculations on the $BaZrS_3$ system are carried out based on density functional theory using the generalized gradient approximation (GGA) with Perdew-Burke-Ernzerhof (PBE) functions, as implemented in the Vienna *ab* initio simulation package (VASP), and projector-augmented-wave (PAW) potentials are used together with a plane-wave basis set[13-15]. The self-consistent calculations were carried out with a 7×15×5 k-point mesh[16]. The Broyden-Fletcher-Groldfarb-Shanno (BFGS) scheme is used to perform the cell optimization. To balance accuracy and speed, the plane-wave basis set cutoff was set to 450 eV. The convergence criteria for total energy, max force, max tress, and SCF iterations were 5×10^{-6}eV/atom, 0.01eV/Å, 0.02 GPa, and 5×10^{-7}eV/atom, respectively.

3. Results and discussion

3.1. Structural properties

By performing first-principles calculation of GGA+PBE functional systematically, we adequately relaxed the equilibrium crystal structure up to generate the satisfactory equilibrium lattice parameters *a*, *b*, *c,* as well as cell volumes *V*, and the present optimized equilibrium lattice parameters and cell volumes of $BaZrS_3$ along with the corresponding experimental and other theoretical data are together summarized in Table 1, and compared to experimental and other theoretical results[17-19]. The predicted lattice constants of $BaZrS_3$ are *a*=8.966 Å, *b*=14.949 Å, and c = 4.454 Å, respectively, consistent with experimental findings[18]: *a*=8.962 Å, *b*=14.873 Å, and c = 3.971 Å, (Table 1), as well as previous other theoretical results[19], implying that the theoretical level we used in the calculations are accurate for predicting the structure properties of $BaZrS_3$.

Table 1. The calculated equilibrium structural parameters of Pnam $BaZrS_3$ at ambient pressure. The previous experimental results are also listed.

Method	a_0 (Å)		b_0(Å)	c_0(Å)
$V(Å^3)$				
This work	8.966	14.949	4.454	534.3
[22]Cal.	8.812	14.474	3.911	----
[23]Expt.	8.962	14.873	3.971	528.9

Furthermore, the pressure dependences of the lattice constants as functions of pressure for the orthorhombic $BaZrS_3$ up to 20 GPa are exhibited in Fig. 1. Obviously, the lattice constants decrease with the increasing applied pressures. By fitting these lattice parameters under different pressure with linear equations, the following expressions were obtained: $a = 8.327 - 0.0486P$; $b = 14.425 - 0.0672P$; $c = 4.587 - 0.008P$; The slopes of fitting linear equations for the lattice parameters *a*, *b* and *c* as a function of pressure were -0.0486 Å /GPa, - 0.0672 Å /GPa, and -0.008 Å /GPa, for *a*, *b* and *c*, respectively. Besides, it was found that when the pressure increased, the lattice parameter *b* decreased the most quickly, followed by *a* and *c*, respectively, indicating that the *b* axis was the most easily compressed while the *c* axis was the most difficult. The sensitivity of axis to compression can be ordered by follow the order of *b* >*a* > *c* axis. This is because, when we increased the pressure then the interaction of Ba, Zr and S atoms becomes stronger and therefore the bond length among these atoms becomes shorter as a result the lattice parameters become smaller with pressure. This similar behavior was often observed in chalcopyrite compound such as $BaMS_3$ (M=Ti and Nb), and $SrZrS_3$[20-21].

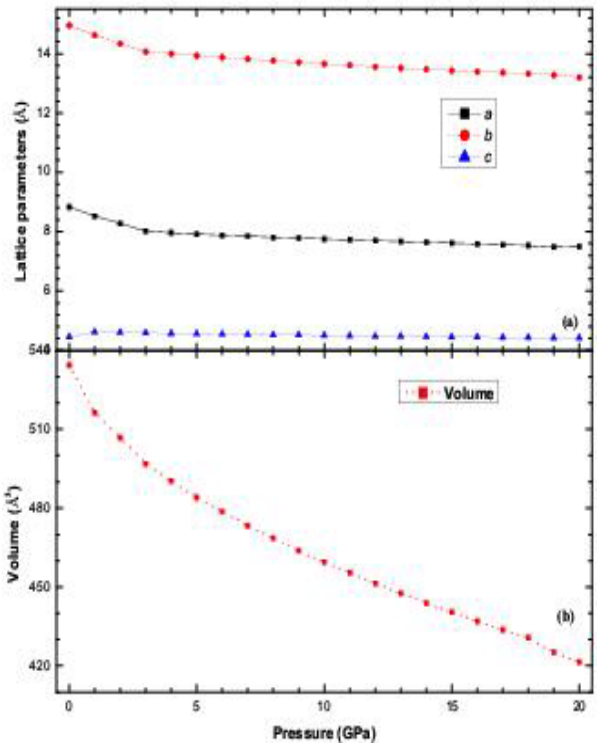

Fig. 1. The lattice constants of the orthorhombic $BaZrS_3$ as a function of pressure.

3.2. Elastic and mechanical properties

To quantify the basic mechanical properties, theoretical elastic constants of $BaZrS_3$ at different pressure are calculated based on strain-stress method. It is well-known that the elastic properties of solid are important to understand its mechanical properties and describe the response when external forces are applied to materials. According to Born's structural stability criteria, elastic constants in the orthorhombic structure must comply with[22]: $C_{11}+C_{22}-2C_{12}>0$; $C_{11}+C_{33}-2C_{13}>0$; $C_{33}+C_{22}-2C_{23}>0$ and $(C_{11}+C_{22}+C_{33}+2C_{12}+2C_{13}+2C_{21})>0$ and $C_{ii}>0$. We calculated the elastic constants of the orthorhombic $BaZrS_3$ in hydrostatic pressures of 0, 5, 10, and 20 GPa. The calculated elastic constants are listed in Table 2. Except for the higher value of C_{11} and C_{33}, the calculated results at zero pressure were very close to the Zhang's calculation values[12], which shows that the elastic constants calculated by GGA+PBE are reliable in this paper. From Table 2, it clearly shows that the calculated elastic constants of $BaZrS_3$ with Pnam symmetry satisfy the criteria, which indicates that they are mechanically stable over the pressure range of 0 to 20 GPa. Moreover, we investigated the pressure effect of elastic constants of the orthorhombic $BaZrS_3$, as illustrated in Fig. 2. To the best of our knowledge, no experimental and theoretical are available. It can be seen that the elastic constant C_{13}, C_{12}, C_{22}, C_{23}, C_{11}, and C_{33} increase monotonically with the increasing pressure. The elastic constant C_{44} increase firstly and then decrease as pressure increases. However, the elastic constants C_{66} and C_{55} have little change with the increasing pressure. It shows that C_{33} and C_{22} both increase monotonically with pressure increasing. But C_{13} increases slowly at first, then it begins to gradually reduce when the pressure reaches 20 GPa.

Table 2. The calculated elastic constants of the orthorhombic $BaZrS_3$ under zero pressure together with other theoretical values[23].

Pressure	C_{11}	C_{22}	C_{33}	C_{44}	C_{55}	C_{66}	C_{12}	C_{13}	C_{23}
0 GPa	79.5	94.4	169.1	30.7	26.9	21.4	48.5	24.1	23.9
[23]Cal.	58.5	114.1	86.4	31.6	27.6	40.5	32.7	42.6	27.9
5 GPa	93.6	128.1	226.1	42.8	37.6	38.9	57.5	35.5	37.1
10 GPa	130.4	143.8	263.9	50.1	52.5	40.87	81.8	50.9	44.2
20 GPa	174.8	182.3	347.6	58.3	78.7	45.6	109.3	75.3	78.8

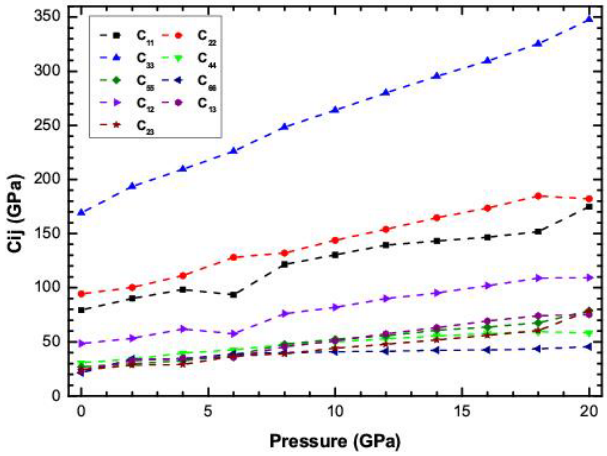

Fig. 2. The elastic constants of the orthorhombic $BaZrS_3$ as functions of pressures.

Furthermore, according to the study of sin'ko et al. the elastic constants of a crystal under pressure are known as: $C'_{\alpha\alpha} = C_{\alpha\alpha} - P$, $C'_{\alpha\beta} = C_{\alpha\beta} + P$ $(\alpha = 1, 2, \dots, 6;\ \beta = 1, 2, \dots, 6)$. Hence, for orthorhombic crystals under pressure, the mechanical stability requires that the elastic constants satisfy the following stability criteria[23]: $C_{ii} - P > 0$, $(C_{11} + C_{22} + C_{33} + 2C_{12} + 2C_{13} + 2C_{23} + 3P) > 0$, and $C_{11} + C_{22} - 2C_{12} - 4P > 0$; $C_{11} + C_{33} - 2C_{13} - 4P > 0$; $C_{22} + C_{33} - 2C_{23} - 4P > 0$. Fig. 3 shows the mechanical stabilities of the orthorhombic $BaZrS_3$ as a function of pressure. Clearly, the values of $C_{11} + C_{22} - 2C_{12} - 4P$ decreases slowly with the increase of pressures, while the value of $C_{22} + C_{33} - 2C_{23} - 4$ and $C_{11} + C_{33} - 2C_{13} - 4$ increases comparatively rapidly. And the calculated results for all satisfy the above stability criteria over the hole pressure range investigated, implying that the structure is mechanically stable within 20 GPa.

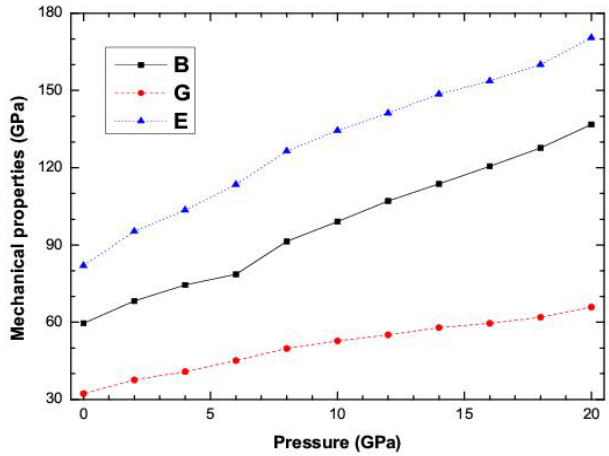

Fig. 3. The mechanical stabilities of the orthorhombic $BaZrS_3$ as a function of pressure.

To further estimate its elastic properties, the multiple elastic modulus of the orthorhombic $BaZrS_3$, bulk modulus (B), shear modulus (G), Young's modulus (E) and Poisson's ratio (δ), are calculated using the Voigt-Reuss-Hill approximation. Based on the elastic constants, the

polycrystalline elastic moduli can be calculated using the Voigt-Reuss-Hill (VRH) method[24-26]. For a orthorhombic structure, the relevant equations are given as follows: $G_R = \frac{15}{4(S_{11}+S_{22}+S_{33})-4(S_{12}+S_{23}+S_{23})+3(S_{44}+S_{55}+S_{66})}$, $G_V = \frac{1}{15}(C_{11} + C_{22} + C_{33} - C_{12} - C_{13} - C_{23}) + \frac{1}{5}(C_{44} + C_{55} + C_{66})$, $G = \frac{1}{2}(G_R + G_V)$, $B_R = \frac{1}{(S_{11}+S_{22}+S_{33})+2(S_{12}+S_{13}+S_{23})}$, $\mathrm{B_V} = \frac{1}{9}(\mathrm{C_{11}} + \mathrm{C_{22}} + \mathrm{C_{33}}) + \frac{1}{9}(\mathrm{C_{12}} + \mathrm{C_{13}} + \mathrm{C_{23}})$, $\mathrm{B_R} = \frac{1}{(\mathrm{S_{11}}+\mathrm{S_{22}}+\mathrm{S_{33}})+2(\mathrm{S_{12}}+\mathrm{S_{13}}+\mathrm{S_{23}})}$, $\mathrm{B} = \frac{1}{2}(\mathrm{B_R} + \mathrm{B_V})$, $E = \frac{9BG}{G+3B}$. where S_{ij} are the inverse matrix of the elastic constants matrix C_{ij}. The calculated results of orthorhombic $BaZrS_3$ under pressure up to 20 GPa are shown in Fig. 4. It is shown that B and E of orthorhombic $BaZrS_3$ increase rapidly with the increasing pressure. As can be seen, the value of bulk modulus B and shear modulus G at 20 GPa is 2.29 and 2.08 times greater than that at 0 GPa, respectively. Additionally, B is larger than G, indicating the parameter limiting stability of the compound is shear modulus[27]. For the sake of exploring the ductile and brittle manner, we checked the pressure dependences of the ratio of bulk modulus to shear modulus (B/G). The value of B/G is associated with ductility or brittleness of a material. If $B/G > 1.75$, the material behaves in a ductile manner. Otherwise, the material exhibits in a brittle manner[28]. In our calculations, the value of B/G for orthorhombic $BaZrS_3$ at 0 GPa is about 1.85, showing that the compound is ductile. And with the increasing pressure, the value of B/G becomes more and more greater. When the pressure up to 20 GPa, the value of B/G is about 2.08, implying pressure can improve the ductility of the orthorhombic $BaZrS_3$. Also, the calculated results have also demonstrated the ductility of this compounds is more and more prominent with increasing applied pressure, it exhibits good mechanical toughness under high pressure.

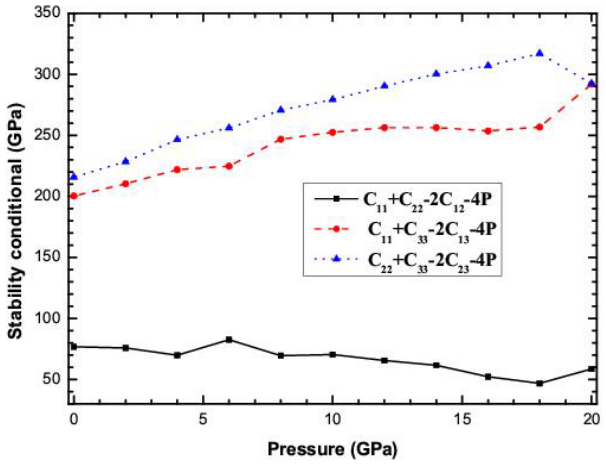

Fig. 4. The elastic moduli B, G, and E of the orthorhombic $BaZrS_3$ as a function of pressure.

3.3. Electronic properties

The effects of pressure on energy bands of the orthorhombic $BaZrS_3$ based on the GGA+PBE are calculated and are depicted in Fig. 5. In the band structure, the dot-line presents the Fermi level. The band structure calculations have been carried out following a path along the

highest symmetry points G, Z, T, Y, S, X, U, and R. The internal coordinates of these points are (0, 0, 0), (0, 0, 0.5), (-0.5, 0, 0.5), (-0.5, 0, 0), (-0.5, 0.5, 0), (0, 0.5, 0), (0, 0.5, 0.5), and (-0.5, 0.5, 0.5) in the first Brillouin zone, respectively. It can be noted that the band structure curves do not pass through the Fermi level and the band gap is 1.75 eV, which indicates that the orthorhombic $BaZrS_3$ is a semiconductor under the pressure of 0 GPa. Both the valence band maximum (VBM) and the conduction band minimum (CBM) are located at the high symmetry G point. It means that $BaZrS_3$ is a direct band gap material. The obtained band gap of 1.75 eV is in consistence with the experimental data of the 1.78 eV reported by Nelson[12].

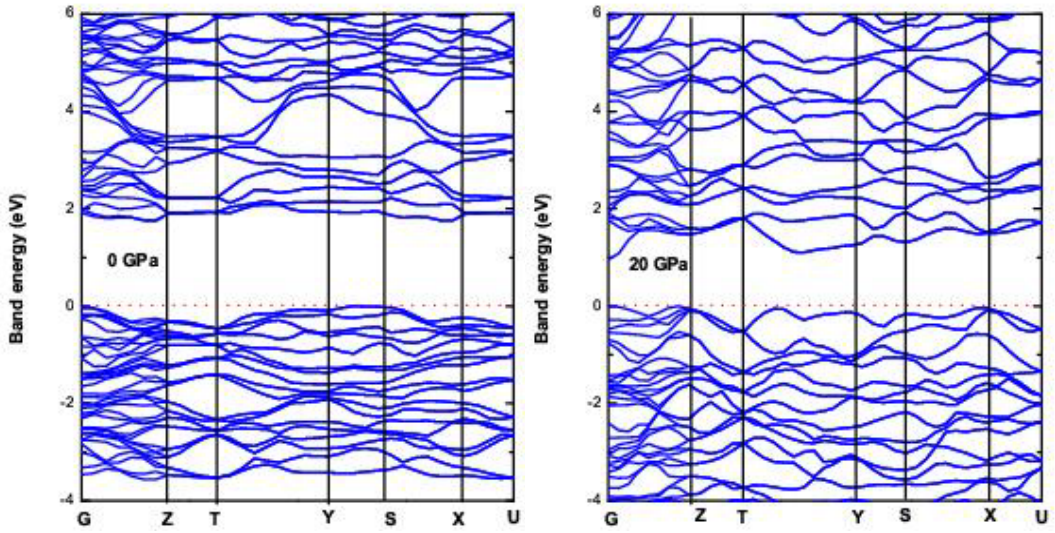

Fig. 5. The band structures of the orthorhombic $BaZrS_3$ at 0 GPa, 10 GPa, and 20 GPa, respectively. The red dashed line is marked the Fermi level.

In order to obtain the pressure effect on the electronic properties of $BaZrS_3$, we have calculated the total density of states and the partial density of states at specific pressures presented in Fig. 6. It can be seen from Fig. 6 that the curve shape of PDOS with the increasing pressure shows no apparent change, meaning a stable $BaZrS_3$ structure and no structural phase transformation in the considered pressures. However, as the pressure increases, the conduction and valence band shift to lower and higher energies, respectively. The shifts of the conduction and valence band result in a decreasing band gap. The reason for this is likely to be that the distance between the atoms decreases under the effect of high pressure, which leads to a change in the atomic orbitals occupied by electrons, which results in the appearance of new hybridizations between different elements. From figure 6, we can observe that above the Fermi level, the total electronic density of states in the conduction band is mainly contributed from the 3p orbital electrons of S atom. In the valence band from -4 to 0 eV, the total electronic density of states is mainly contributed with hybrid characteristics and mainly consisted of S 3S orbital and a small amount of Zr 5s and 4d orbitals. The contribution of the Ba atomic orbital to VBM and CBM is very weak and even negligible. The Zr 4d orbital and S 3p orbital anti-bonding interactions were very strong, indicating that the change of CBM played a leading role in the narrowing of the band gap. This change in the density of states is a concrete manifestation of changes in the band structure and band gap of the $BaZrS_3$ system. That is to say, due to the decrease of lattice constants

under high pressure, the atoms become closer to each other, which leads to the decreased free orbit spacing between the outer valence electrons of each atom, the enhanced interaction between them, and thus the decreased band gap. Moreover, the pressure response of the band gap and electrical conductivity is vitally significant for practical applications and may guide in photoelectric device design[29].

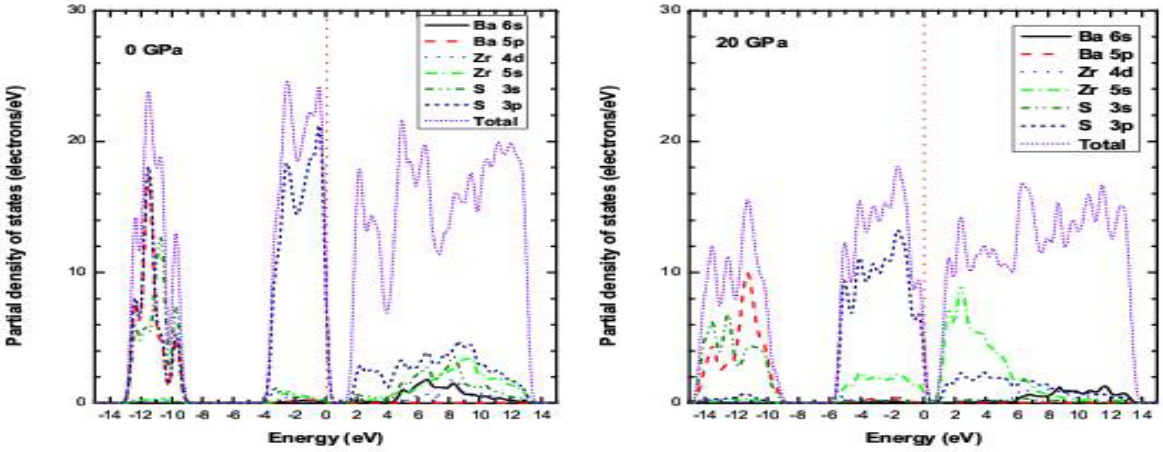

Fig. 6. The density of state (DOS) and partial density of state (PDOS) of the orthorhombic $BaZrS_3$ at 0 GPa, 10 GPa, and 20 GPa, respectively. The red dashed line is marked the Fermi level.

4. Conclusions

In this work, DFT calculations have been performed to study the structural, and electronic properties of the chalcopyrite semiconductor $BaZrS_3$ in the pressure range of 0-20 GPa. Structural parameters are found to compare well with the available data in the previous reports. Elastic constants and their dependence on pressure and related mechanical properties have been reported. From the quotient of bulk to shear modulus of B/G, it is found that ductility becomes stronger with the increasing pressure, indicating pressure can effectively improve the ductility of the orthorhombic $BaZrS_3$. We believe that the consistency between the mechanical and electronic quantities encourages us to further experimental investigations to verify the theoretical findings, and importantly to look for a possible optoelectronic device in this material.

References

[1] S. Perera, H. Hui, C. Zhao, H. Xue, F. Sun, C. Deng, N. Gross, C. Milleville, X. Xu, D. F. Watson, B. A. Weinstein, Y. Y. Sun, S. Zhang, and H. Zeng, Nano Energy 22, 129 (2016); https://doi.org/10.1016/j.nanoen.2016.02.020

[2] S. Niu, H. Huyan, Y. Liu, M. Yeung, K. Ye, L. Blankemeier, T. Orvis, D. Sarkar, D. J. Singh, R. Kapadia, and J. Ravichandran, Adv. Mater. 29, 1604733 (2017). 3T. Zhang, M. Yang, Y. Zhao, K. Zhu, Nano Lett. 15, 3959 (2015); https://doi.org/10.1002/adma.201604733

[3] C. Bi, Q. Wang, Y. Shao, Y. Yuan, Z. Xiao, J. Huang, Nat. Commun. 6, 7747 (2015); https://doi.org/10.1038/ncomms8747

[4] W. Nie, H. Tsai, R. Asadpour, J. C. Blancon, A. J. Neukirch, G. Gupta, J. J. Crochet, M. Chhowalla, S. Tretiak, M. A. Alam, H. L. Wang, A. D. Mohite, Science 347, 522 (2015);

https://doi.org/10.1126/science.aaa0472
[5] W. Meng, B. Saparov, F. Hong, J. Wang, D. B. Mitzi, and Y. Yan, Chem. Mater. 28, 821 (2016); https://doi.org/10.1021/acs.chemmater.5b04213
[6] U. Schwarz, F. Wagner, K. Syassen, H. Hillebrecht, Phys. Rev. B: Condens. Matter Mater. Phys. 53, (1996) 12545; https://doi.org/10.1103/PhysRevB.53.12545
[7] M. Szafrański, A. Katrusiak, J. Phys. Chem. Lett. 8, (2017) 2496; https://doi.org/10.1021/acs.jpclett.7b00520
[8] S. Niu, J. M. Guerrero, Y. Zhou, K. Ye, B. Zhao, B. Melot, J. Ravichandran, J. Mater. Res. 33, 4135 (2018); https://doi.org/10.1557/jmr.2018.419
[9] K. Kuhar, M. Pandey, K. S. Thygesen, K. W. Jacobsen, ACS Energy Lett. 3, 436 (2018); https://doi.org/10.1021/acsenergylett.7b01312
[10] S. Niu, G. Joe, H. Zhao, Y. Zhou, T. Orvis, H. Huyan, J. Salman, K. Mahalingam, B. Urwin, J. Wu, Y. Liu, T. E. Tiwald, S. B. Cronin, B. M. Howe, M. Mecklenburg, R. Haiges, D. J. Singh, H. Wang, M. A. Kats, J. Ravichandran, Nat. Photon. 12, 392 (2018); https://doi.org/10.1038/s41566-018-0189-1
[11] Y. Li, D. J. Singh, Eur. Phys. J. B 91, 188 (2018).
[12] G. Nelson, Y. Y. Sun, S. Perera, H. L. Hui, X. C. Wei, S. B. Zhang, H. Zeng, and B. A. Weinstein, Phys. Rev. Applied. 8, 044014 (2017).
[13] N. D. Mermin, Phys. Rev., 137(5A), A1441 (1965); https://doi.org/10.1103/PhysRev.137.A1441
[14] J. Hafner, J. Comput. Chem., 29(13), 2044 (2008); https://doi.org/10.1002/jcc.21057
[15] J. P. Perdew, A. Zunger, Phys. Rev. B 23, (1981) 5048; https://doi.org/10.1103/PhysRevB.23.5048
[16] H. J. Monkhorst, J. D. Pack, Phys. Rev. B. 3, 5188 (1976); https://doi.org/10.1103/PhysRevB.13.5188
[17] R. Lelieveld, D.J. Ijdo, Acta Crystallogr. B36, 2223 (1980); https://doi.org/10.1107/S056774088000845X
[18] R. Lelieveld and D. J. W. IJdo, Acta Crystallogr., Sect. B: Struct. Crystallogr. Cryst. Chem., 36(10), 2223 (1980); https://doi.org/10.1107/S056774088000845X
[19] O. A. Eric, N. Koratkarb and G. Balasubramanian, J. Mater. Chem. C, 9, 3892 (2021); https://doi.org/10.1039/D1TC00374G
[20] M. Ishii and M. Saeki, Phys. Status Solidi B 170, K49 (1992); https://doi.org/10.1002/pssb.2221700149
[21] M. Ishii, M. Saeki, and M. Sekita, Mater. Res. Bull. 28, 493 (1993); https://doi.org/10.1016/0025-5408(93)90132-W
[22] Wu Z. J, Hao X. F, Liu X. J, Meng J, Phys. Rev. B 75, 054115 (2007).
[23] G. V. Sin'ko, N. A. Smirnov, J. Phys. Condens. Matter 14, 6989 (2002); https://doi.org/10.1088/0953-8984/14/29/301
[24] Z. Wu, E. Zhao, H. Xiang, X. Hao, X. Liu, J. Meng, Phys. Rev. B 76, 054115 (2007).
[25] J. I. Tani, M. Takahashi, H. Kido, Comp. Mater. Sci. 50, 2009 (2011); https://doi.org/10.1016/j.commatsci.2011.01.053
[26] M. Mattesini, S. F. Matar, Phys. Rev. B 65, 075110 (2002).
[27] I. R. Shein, A. L. Ivanovskii, J. Phys. Condens. Mater. 20, 415218 (2008); https://doi.org/10.1088/0953-8984/20/41/415218
[28] P. Ravindran, LarsFast, P. A. Korzhavyi, B. Johansson, J. Wills, O. Eriksson, J. Appl. Phys. 84, 4891 (1998); https://doi.org/10.1063/1.368733
[29] S. Saha, T. P. Sinha, and A. Mookerjee, Phys. Rev. B 62, 8828 (2000); https://doi.org/10.1103/PhysRevB.62.8828